Four-component united-atom model of bitumen

J. S. Hansen,[1,a)] Claire A. Lemarchand,[1] Erik Nielsen,[2] Jeppe C. Dyre,[1] and Thomas Schrøder[1]

[1]*DNRF Centre "Glass and Time", IMFUFA, Department of Science, Systems and Models, Roskilde University, Postbox 260, DK-4000 Roskilde, Denmark*

[2]*Danish Road Directorate, Guldalderen 12, DK-2640 Hedehusene, Denmark*

(Received 29 November 2012; accepted 30 January 2013; published online 7 March 2013)

We propose a four-component united-atom molecular model of bitumen. The model includes realistic chemical constituents and introduces a coarse graining level that suppresses the highest frequency modes. Molecular dynamics simulations of the model are carried out using graphic-processor-units based software in time spans in order of microseconds, which enables the study of slow relaxation processes characterizing bitumen. This paper also presents results of the model dynamics as expressed through the mean-square displacement, the stress autocorrelation function, and rotational relaxation. The diffusivity of the individual molecules changes little as a function of temperature and reveals distinct dynamical time scales. Different time scales are also observed for the rotational relaxation. The stress autocorrelation function features a slow non-exponential decay for all temperatures studied. From the stress autocorrelation function, the shear viscosity and shear modulus are evaluated, showing a viscous response at frequencies below 100 MHz. The model predictions of viscosity and diffusivities are compared to experimental data, giving reasonable agreement. The model shows that the asphaltene, resin, and resinous oil tend to form nano-aggregates. The characteristic dynamical relaxation time of these aggregates is larger than that of the homogeneously distributed parts of the system, leading to strong dynamical heterogeneity. [http://dx.doi.org/10.1063/1.4792045]

I. INTRODUCTION

Refined bitumen (or asphalt) is a residual product of the refinery process of crude oil and is highly viscous at room temperature. The chemical composition of bitumen is very complex in that it is composed of up to 10^6 different types of molecules,[1–4] typically with molar masses above 200 g/mol. Bitumen is not chemically unique in the sense that its composition depends on the crude oil source, the age of the bitumen,[5] and possible chemical modifiers.[6] The functional chemistry includes heteroatoms such as sulfur and nitrogen, cyclic structures, aromatics compounds, and saturated hydrocarbons,[5] and these enter larger and complicated molecular structures. A correct and detailed chemical categorization is not feasible, and bitumen is often characterized simply by its rheological properties such as bulk and shear moduli or penetration depth;[7] the latter is a standard method used in the road pavement industry. A fundamental understanding on the molecular level is, however, necessary if one wishes to understand and control the mechanical properties.

The aim of the present work is to do just that, i.e., we wish to study dynamical properties of bitumen through molecular modelling. A further impetus of this work lies on the definition and characterization of a "Cooee-bitumen model" with the aim to bring new insights on how to reduce the rolling resistance generated between the tyre and the pavement.[8] Molecular simulations have previously been used to investigate bitumen properties, for example, the density and structure in asphaltene systems[2] and molecular alignment.[4] Recently, Zhang and Greenfield (Z & G) published a series of papers,[6,9–12] wherein they study structural, thermodynamical, and dynamical properties of different bitumen models with and without polymer additives. To this end the authors used atomistic molecular dynamics simulations. Their bitumen models are based on a tertiary mixture in which each chemical component represents a distinct constituent: high-weight asphaltenes, aromatic maltenes (resin), and saturated maltenes (*n*-alkanes). In their simulations, they applied an all-atom force-field that includes the interactions between both hydrogen and carbon and hydrogen and sulfur, as well as the hydrogen-carbon bonds. While this allows for standard and well tested force field parameterizations and gives very detailed description of the system, it also includes very fast modes, which are unlikely to couple to the long relaxation times characterizing viscous liquids like bitumen. The inclusion of these fast modes necessitates a small integration time step in the numerical integration of Newton's equations of motion, and Z & G were only able to simulate a time span in the order of 10 ns, even when using parallelized molecular dynamics software.[12] For the aromatic maltene constituent, Z & G used dimethylnaphthalene or closely related molecular structures. This relatively low weight molecule has a boiling point of around 278 °C[13] and is therefore likely to be removed from the crude oil during the refinery process at approximately 500 °C, see Ref. 5.

We propose a new four-component "Cooee-bitumen" model, based on the Hubbard-Stanfield classification.[14,15] The model is coarse grained such that the hydrogen atoms

a)jschmidt@ruc.dk.

are not explicitly included, but implicitly through parameterization of the particle interactions. This united atomic unit approach, see, e.g., Ref. 16, allows for larger time steps and, more importantly, it reduces significantly the number of bond-, angle-, and pair-forces to be evaluated in each time step. The molecular dynamics simulations are carried out using the Graphical-Processor-Unit (GPU) based molecular dynamics software package RUMD[17] version 1.2. In this way time spans in the order of μsec are accessible using a single graphics card. We are thus able to study much slower relaxation phenomena in bitumen than was previously possible.

In this first paper we focus on the dynamical properties of the model and identify the temperature where the relaxation time becomes very long compared to the time scales that can be simulated. Specifically, we investigate characteristic relaxation times for collective, chemical and single molecule quantities. From this, we show that the dynamical properties of the model are quite different from those of Z & G's model, in that the dynamics is much slower. For relatively low temperatures, the dynamics is characterized by complex glass-like behavior, where the relaxation times widely exceed the accessible simulation times.

The paper is organized as follows. Section II describes the parameters chosen in the model and the simulation method. Section III contains results and discussion of diffusivity, viscous properties, and rotational dynamics of the model bitumen. Finally, a summary is provided in Sec. IV.

II. MODEL, PARAMETERIZATION, AND METHODOLOGY

As stated in the introduction, a detailed chemical model for bitumen is not realistic. We do therefore not target any specific bitumen, but aim at capturing the characteristic properties of a typical bitumen. We conjecture that an explicit inclusion of the hydrogen atoms is not important for this modelling purpose, even if it may be useful for other specific purposes (see, for example, Ref. 16). We therefore coarse grain the chemical structures, making it possible to investigate longer time dynamics.

A. Parameterization

The bitumen constituents are characterized using different separation techniques.[5,7,18] Here we use the general classification scheme of Hubbard and Stanfield,[14,15] see Fig. 1. We let unsaturated hydrocarbons and the aromatic/cyclic compounds without any heteroatoms like sulfur fall into the category resinous oils.[5] Also, we interpret the class non-resinous oils to be paraffin wax, i.e., saturated hydrocarbons. This motivates a four-constituent model composed of

1. Asphaltene.
2. Resin.
3. Resinous oil.
4. Saturated hydrocarbon.

The model follows the SARA (Saturates-Aromatics-Resins-Asphaltenes) classification,[19] although the unsaturated hydrocarbons and the aromatic/cyclic compounds fall under the category "Aromatics" in the SARA classification, we prefer to use the term resinous oil to follow Hubbard and Stanfield.[14,15]

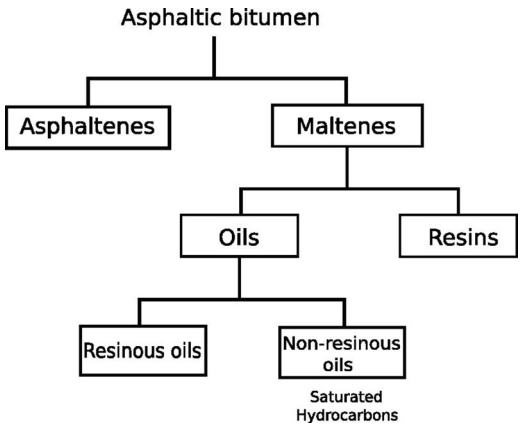

FIG. 1. Bitumen classification scheme of Hubbard and Stanfield.[14,15]

A single type of molecule represents each constituent. Based on Nuclear Magnetic Resonance (NMR) studies Artok[3] proposed an asphaltene structure, shown in Fig. 2, which is adopted here. This structure was also used by Z & G, termed asphaltene 1. For the resinous oil and resin, we use the structures by Rossini *et al.*[20] and Murgich *et al.*,[4] respectively. In Ref. 9, Z & G argued that the saturated hydrocarbons can be modelled by docosane (n-C_{22}), since this molecule represents the average chain length found by Storm *et al.*[21] this molecule is also used here. All four molecular structures are shown in Fig. 2.

We represent the methyl (CH_3), methylene (CH_2), and methine (CH) groups by the same Lennard-Jones particle, a united atomic unit (UAU) with mass 13.3 g/mol and Lennard-Jones parameters $\sigma = 3.75$ Å and $\epsilon/k_B = 75.4$ K. These parameters are estimated from the Optimized Potentials for

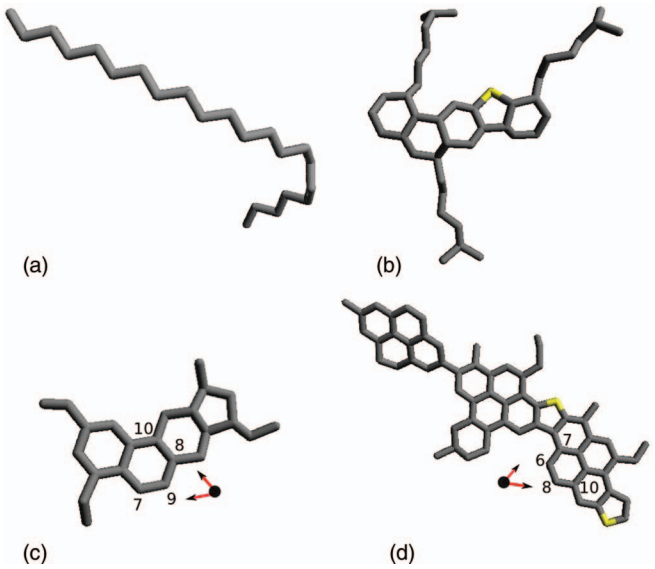

FIG. 2. United-atom-unit models of the constituent molecules in the "Cooee-bitumen" model. (Top left) Docosane. (Top right) Resin. (Lower left) Resinous oil. (Lower right) Asphaltene. Yellow indicates sulfur atoms. Numbers and arrows identify bond-vectors used in the data analysis, see text for details.

Liquid Simulations (OPLS) force field.[22] The sulfur atoms are represented by the same Lennard-Jones interaction, but with a mass of 32 g/mol. For this particular choice of parameters, the sulfur atoms and the carbon-based UAUs are chemically identical, i.e., the molecules do not possess any polarity; however, polarity can easily be included into the model if one wishes so.

The force field is given through the following total potential energy of the system

$$U(\mathbf{r}) = \sum_i \sum_{j>i} 4\epsilon \left[\left(\frac{\sigma}{r_{ij}} \right)^{12} - \left(\frac{\sigma}{r_{ij}} \right)^{6} \right] + \frac{1}{2} \sum_{\text{bonds}} k_s (r_{ij} - l_b)^2 + \frac{1}{2} \sum_{\text{angles}} k_\theta (\cos\theta - \cos\theta_0)^2 + \sum_{\text{dihedrals}} \sum_{n=0}^{5} c_n \cos^n \phi. \quad (1)$$

The force field thus includes pair interactions, as well as interactions due to (flexible) bonds, angles, and dihedral angles. The bonds, angles, and dihedral angles are specified via bonds between the UAUs. UAUs belonging to the same bond, angle, or dihedral angle do not interact via the pair interaction.

From the force field, it can be seen that the model has a large parameter space. To reduce the number of free parameters, we assume that all bonds have the same length $l_b = 1.46$ Å. This particular value of l_b is chosen as it is the average value of all the bonds in the system (1.46 ± 0.07 Å) computed from energy minimization of the individual molecules.[23] This is, of course, a simplification since energy minimization of, for example, the asphaltene molecules gives the single-bonded units a bond length of around 1.50–1.54 Å and the double-bonded units a bond length of 1.38–1.41 Å. These values again depend on the specific molecule and amount to many different bond lengths, so we choose an average value for simplicity. The same argument lies behind the choices of the angles and dihedral angles, but here we use two distinct angles and three distinct dihedral angles. The choice of bond length and angles increases the aromatic regions and decreases the length of the aliphatic parts of the systems. As our aim is to propose a simple model characterizing the dynamical properties of bitumen in general, we believe this simplification is appropriate.

We use the Generalized Amber Force Field (GAFF)[24] parameterization for bond and angle parameters, see Table I. For the saturated hydrocarbons and the side chains in the asphaltene and resin, we use the Ryckaert-Bellemans parameters.[25] These parameters are optimized with respect to liquid butane, but they capture the important *cis*, *trans*, and *gauche* configurations reasonably well. We are thereby left with a single free parameter, namely, the zero-force coefficient c_1 for dihedral angles $\phi = 180°$ and $0°$ in the ring structures.

The c_1 parameter is estimated from one structural criterion, namely, the alignment between the aromatic rings in a one-component system of 1,7-dimethylnaphthalene (also used by Z & G). This particular criterion is chosen because of the simple molecular structure of 1,7-dimethylnaphthalene. Let the vector $\mathbf{u}_1$ be defined as the cross product $\mathbf{u}_1 = \mathbf{r}_1 \times \mathbf{r}_2$, where $\mathbf{r}_1$ and $\mathbf{r}_2$ are two vectors parallel with two bonds in one of the ring structures of the molecule, as shown in Fig. 3. Thus, $\mathbf{u}_1$ is a vector normal to the ring structure. Likewise, the vector $\mathbf{u}_2$ is defined as normal to the second ring structure. The angle between $\mathbf{u}_1$ and $\mathbf{u}_2$ then defines the ring alignment angle, $\theta = \cos^{-1}(\mathbf{u}_1 \cdot \mathbf{u}_2 / |\mathbf{u}_1||\mathbf{u}_2|)$. Figure 3 shows the histogram of the alignment angle for 1,7-dimethylnaphthalene at mass density 994 kg/m^3 and temperature $T = 358.15$ K. The values $c_1 = 20$ kcal/mol and $c_1 = -20$ kcal/mol were chosen for the $\phi = 180°$ and $\phi = 0°$ zero-force dihedral angles, respectively, since they lead to a good agreement between the all-atom model used by Z & G and the present united-atom model.

TABLE I. Force-field parameters of the "Cooee-bitumen" model, see Eq. (1).

Bonds	l_b (Å)	k_s (kcal/mol)
All	1.46	403
Angles	θ_0 (deg)	k_θ (kcal/(mol rad^2))
Aromatic/cyclo	120	108
Aliphatic	106	70
Dihedrals	Angle (deg)	c_n (kcal/mol)
Aromatic/cyclo	180	20 (n = 1)
Aromatic/cyclo	0	−20 (n = 1)
Linear/aliphatic		Ryckaert-Belleman

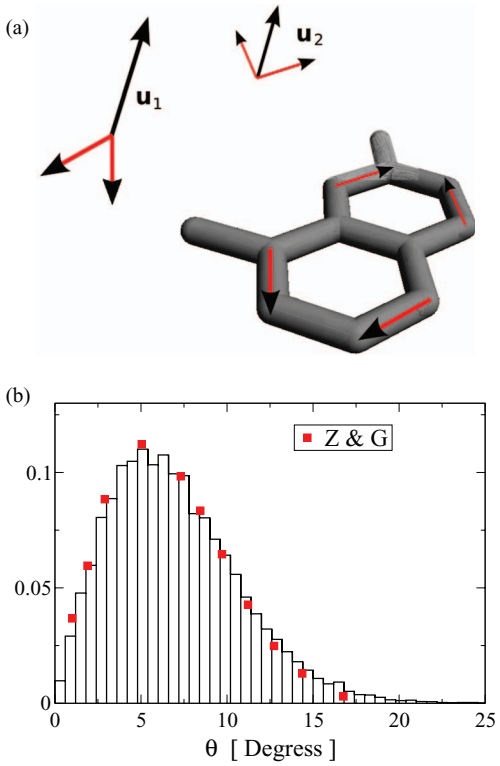

FIG. 3. (a) Definition of the alignment angle, θ, in 1,7-dimethylnaphthalene. (b) Simulation data for the angle distribution of pure 1,7-dimethylnaphthalene at the state point $\rho = 994$ kg/m^3 and $T = 358.15$ K. Reference data are taken from Ref. 10.

B. Simulation method

In all simulations we use $N_A = 10$ asphaltene, $N_R = 10$ resin, $N_{RO} = 10$ resinous oil, and $N_D = 82$ docosane molecules, giving a total of 3114 UAUs. This mass fraction corresponds closely to Z & G's mixture 1,[9] for which dimethylnaphthalene represents both the resin and resinous oil, but we use twice as many molecules. Initially, the molecules' centers-of-masses are arranged on a simple low-density lattice and the system is compressed to the desired density while integrating the equations of motion. We use a target density of $\rho = 994$ kg/m^3, and the quench is carried out at temperature $T = 603$ K. The system was coupled to a Nosé-Hoover thermostat[26,27] and the equations of motion were integrated using a leap-frog integrator scheme.[28] After compression, the volume is kept fixed in order to perform NVT ensemble simulations. A first production run is carried out at $T = 603$ K over a total time span of 0.85 μsec. During this run the system reaches equilibrium (see the discussion below). The final configuration from this simulation is used to reduce the temperature from $T = 603$ K to $T = 528$, 490, and 452 K, respectively, at a rate of 2.2 K/ns. In this way we studied the systems at four different temperatures. The state points chosen in this work, of course, do not represent operational conditions of bitumen. However, the temperature 452 K is not much higher than the temperature at which bitumen, filler, and stones are processed and mixed, which is at 420–430 K for the 70/100 standard bitumen.[29] For $T \leq 528$ K, production runs of 1.7 μsec were performed. For all temperatures the production runs were divided into 10 time intervals of identical length (0.085 μsec and 0.17 μsec for $T = 603$ K and $T \leq 528$ K, respectively). This enables us to follow the equilibration of the system. In order to avoid the initial fast relaxations in the system, we only used the last eight sample intervals for data analysis.

To highlight the different dynamics, we also study the system at a relatively low temperature and far from equilibrium. To this end, a dilute and high-temperature system is rapidly quenched to the target density and $T = 301$ K. This system was also simulated over a time span of 1.7 μsec.

Since the density is fixed in all simulations, the pressure is not constant. Thus, for $T = 301$ K the pressure is $(2 \pm 2) \times 10^2$ MPa, whereas for $T = 603$ K the pressure is $(25 \pm 4) \times 10^2$ MPa, which is above ambient pressure.

To determine an acceptable integration time step, the energy drift was investigated by performing a series of NVE simulations over one million time steps at the desired density for different temperatures. For low temperatures and time steps larger than 3.4 fs, we noticed a slight systematic increase in the energy fluctuations (quantified by the energy standard error). To be conservative, we chose a time step of 1.7 fs for $T \leq 528$ K and 0.85 fs for T = 603 K. These time steps are around 35%–70% larger than those used by Z & G,[11] which is made possible by the coarse graining. This enables us to simulate a time span of up to 1.7 μsec using one billion time steps, which is possible by the usage of the GPU. This takes approximately 10 days on a NVIDIA GTX-480 graphics card.

III. RESULTS AND DISCUSSION

This section analyzes (i) the average diffusivity of the four different chemical components, (ii) the collective viscous properties through the stress (or, equivalently, the pressure tensor) autocorrelation function, and (iii) the orientational dynamics of single resinous oil and asphaltene molecules.

A. Diffusivity

The molecular diffusivity is evaluated through the mean-square displacement of the center-of-mass. If the center-of-mass position of molecule i is denoted $\mathbf{r}_i$, the mean-square displacement of molecules of a certain type is defined as[30] $\langle \Delta \mathbf{r}^2(t) \rangle = \frac{1}{N} \sum_i^N \Delta \mathbf{r}_i^2(t)$, where the index i runs over molecules of identical type. In the normal diffusive regime,

$$\log_{10}[\langle \Delta \mathbf{r}^2(t) \rangle] = \log_{10}(6D) + \log_{10}(t), \tag{2}$$

where D is the diffusion coefficient. In Fig. 4, the mean-square displacements of the four components are plotted for temperatures 452 K and 603 K. The molecules are in the normal diffusive regime at both temperatures for times longer than 1 ns. The corresponding diffusion coefficients are plotted in Fig. 5 for different temperatures. Upreti and Mehrotra[31] reported diffusivities of the order of (0.1–1.0) $\times 10^{-9}$ m^2/s for small weight gases in bitumen over a temperature range of 20–200 °C, which is in reasonable agreement with our results in view of the fact that we study higher weight molecules. From Fig. 5, it follows that $D_D > D_{RO} > D_R > D_A$, where

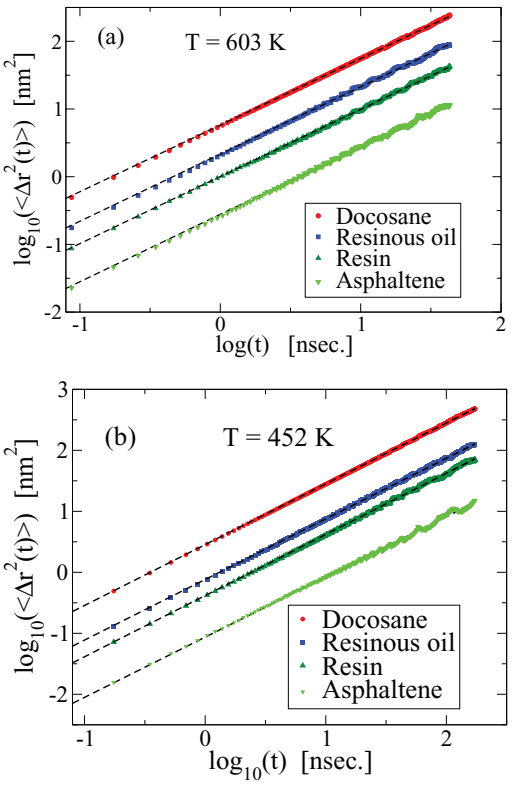

FIG. 4. Mean-square displacement of the molecules. Dashed lines are the best fits of Eq. (2) to the data points, for t smaller than 1.7 ns. (a) $T = 603$ K, (b) $T = 452$ K.

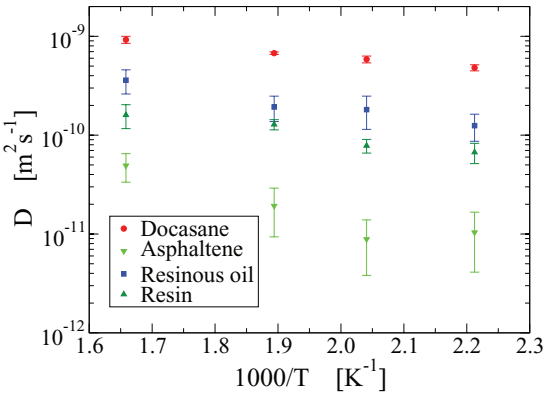

FIG. 5. Arrhenius plot for the four chemical constituents in the bitumen model. The error bars are standard deviations estimated from the eight last sample intervals of each production run.

D_D is the diffusivity for docosane, D_{RO} for resinous oil, D_R for resin, and D_A for asphaltene. This, of course, is consistent with the fact that the mobility decreases with increasing molecular size.

Both asphaltene and docosane have diffusion coefficients that are lower than the values reported by Z & G,[11] who found $D_D = 1 \times 10^{-9}$ m^2/s and $D_A = 2.5 \times 10^{-10}$ m^2/s at $T = 440.5$ K. This discrepancy is likely due to the current model replacing 1,7-dimethylnaptalene with the resin and resinous oil compounds. These relatively large structures hinder the motion of the compounds significantly compared to the smaller 1,7-dimethylnaphthalene. This may also explain another difference between the two models: we find a large difference in diffusivities between the docosane and asphaltene ($D_D \approx 20 D_A$), whereas Z & G's model shows a difference of only a factor of 5.

The mean-square displacement for a system rapidly quenched to the temperature 301 K is also studied and is plotted in Fig. 6. In order to highlight the details (opposed to what was done in Fig. 4), no sample averaging is done here. The docosane molecules still exhibit an approximate diffusive motion, whereas the larger resin and resinous oil molecules perform vibrational motion around a given position (arrested), and then make a rapid movement (jump). The resin molecules eventually enter an approximately diffusive regime. The arrest and jump motions are both random events, which are also observed for simple models of glasses.[32,33] This behavior shows the inherent heterogeneous dynamics present in the model where the asphaltenes are immobile on the time scales shown in the figure, whereas the docosanes approach normal diffusivity.

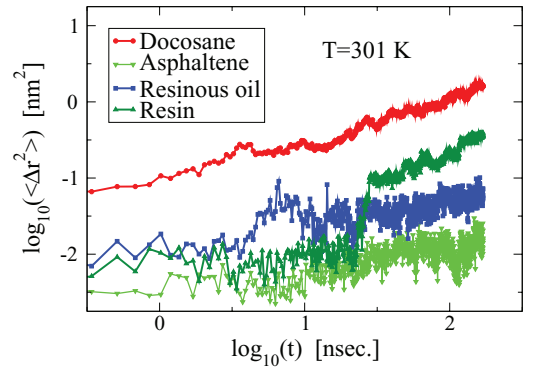

FIG. 6. Mean-square displacement of the molecules for the rapidly quenched system, i.e., in the glass phase. Additional averaging over time lags, as in Fig. 4, was not carried out here to highlight the details.

B. Viscosity

To study the viscous properties we use the Irving-Kirkwood[34] expression for the pressure tensor

$$\mathsf{P} = \frac{1}{V}\sum_i \left[\frac{\mathbf{p}_i\mathbf{p}_i}{m_i} + \sum_{j>i}\mathbf{r}_{ij}\mathbf{F}_{ij}\right], \tag{3}$$

where $\mathbf{p}_i$ is the momentum of molecule i, m_i its mass, $\mathbf{r}_{ij} = \mathbf{r}_i - \mathbf{r}_j$ is the center-of-mass displacement vector between molecules i and j, and $\mathbf{F}_{ij}$ is the total force between molecules i and j. This force is the sum of the atomic forces,[35] i.e., $\mathbf{F}_{ij} = \sum_{\alpha\in i}\sum_{\beta\in j}\mathbf{F}_{\alpha\beta}$, where atom α is an atom in molecule i, and β in molecule j. V is the system volume. The pressure tensor defined above is in general not symmetric;[35] its traceless symmetric part $\overset{\text{os}}{\mathsf{P}}$ can be extracted using $\overset{\text{os}}{\mathsf{P}} = \frac{1}{2}(\mathsf{P} + \mathsf{P}^T) - \frac{1}{3}\text{trace}(\mathsf{P})$. From this, we find the shear stress autocorrelation function via

$$C_P(t) = \frac{1}{3}\sum_{(\alpha\beta)}\langle\overset{\text{os}}{\mathsf{P}}_{(\alpha\beta)}(0)\,\overset{\text{os}}{\mathsf{P}}_{(\alpha\beta)}(t)\rangle, \tag{4}$$

where $(\alpha\beta)$ runs over the xy, xz, and yz pressure tensor elements and $\langle\ldots\rangle$ denotes an ensemble average. The ensemble average is considered equivalent to a time average. Each sample interval is divided into sample windows for C_p with time spans of around 2 ns. The product $\overset{\text{os}}{\mathsf{P}}_{(\alpha\beta)}(t_0)\,\overset{\text{os}}{\mathsf{P}}_{(\alpha\beta)}(t_0+t)$ is computed for a time t, $0 \geq t \geq 2$ ns for different initial times t_0 within the specific window. The average is performed over the initial times within a period and over the different periods, leading to the stress autocorrelation function for times up to 2 ns. Comparing the results of the 8 successive samples in a production run enables us to probe the equilibration process.

In Fig. 7, the stress autocorrelation function is plotted for $T = 603$ K and for $T = 452$ K. For the highest temperature, (Fig. 7(a)) the correlation function is fully decayed (note the logarithmic scale of the x-axis) and time invariant within statistical error, as shown by the equivalent results obtained for different samples. For lower temperatures, e.g., $T = 452$ K in Fig. 7(b), it is seen that the autocorrelation function does not relax fully and that the eight successive samples in a production run do not lead to the same result, i.e., the relaxation time characterizing the collective dynamics is larger than the sample window for the stress autocorrelation function of 0.17 μsec.

For highly viscous liquids, the relaxation processes are often quantified by non-exponential functions,[36] for instance, the stretched exponential function

$$C(t) = C(0)\exp(-(t/\tau_c)^\beta), \tag{5}$$

where τ_c is the characteristic relaxation time and $\beta < 1$. Figure 7 shows the best fits of the form given in Eq. (5) to

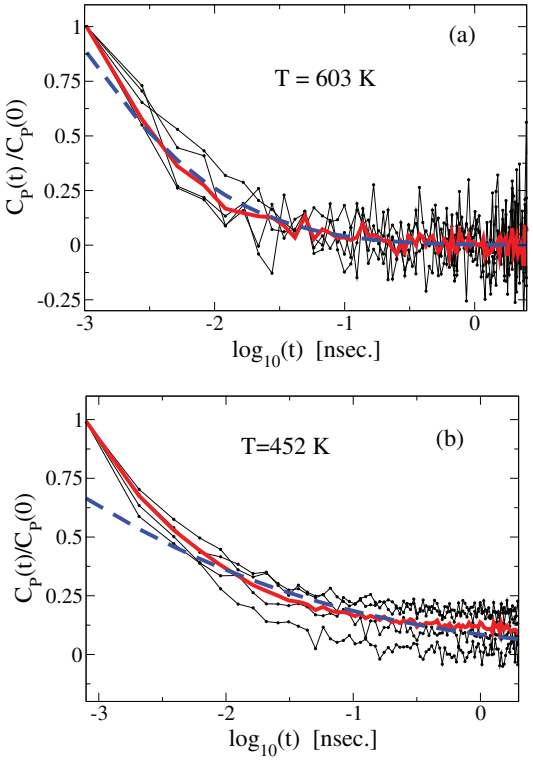

FIG. 7. Normalized stress autocorrelation functions defined in Eq. (4) as a function of time for four samples among the ten successive ones in a production run (dots connected with black lines). Red curves are the average of the last eight sample intervals, blue dashed line is the best fit of the form given in Eq. (5) to the averaged data from 0 to 0.63 ns.

the averaged data (red line). It is seen that the stretched exponential form fits data well even for small times for $T = 603$ K. For this temperature, the coefficient β is around 0.20 which may be interpreted as an indication of strong spatial dynamical heterogeneity.[36] We discuss this point further below.

The frequency-dependent viscosity $\eta^*(\omega) = \eta'(\omega) - i\eta''(\omega)$ is given by the stress autocorrelation function as follows:[30]

$$\eta^*(\omega) = \frac{V}{k_B T} \int_0^\infty C_P(t) \exp(-i\omega t)\, dt. \tag{6}$$

This expression can, of course, only be used for temperatures where the stress autocorrelation function is fully relaxed; in Fig. 8(a) we plot the running integral $I(t) = \int_0^t C_P(s)\, ds$, indicating that this is the case within statistical uncertainty for $T = 603$ K.

Figure 8(b) displays $\eta^*(\omega)$ for $T = 603$ K; it is observed that the fluid response is purely viscous for $\omega < 100$ MHz. The imaginary part of the viscosity exhibits a peak at around 0.5 GHz, which corresponds to a characteristic relaxation time of approximately 2 ns. The frequency-dependent shear modulus $G^*(\omega) = G'(\omega) + iG''(\omega) = i\omega\eta^*(\omega)$ is plotted in Fig. 8(c). Two distinct regimes are clearly observed; at low frequencies $G' \propto \omega^2$, which is the zero-frequency behavior, and at high frequencies $G' \propto \omega^{1/4}$.

In order to be able to calculate the zero-frequency viscosity from Eq. (6) with reasonable accuracy, it is necessary to simulate for much longer times than the Maxwell relaxation time. This is the time that characterizes the long-time decay of

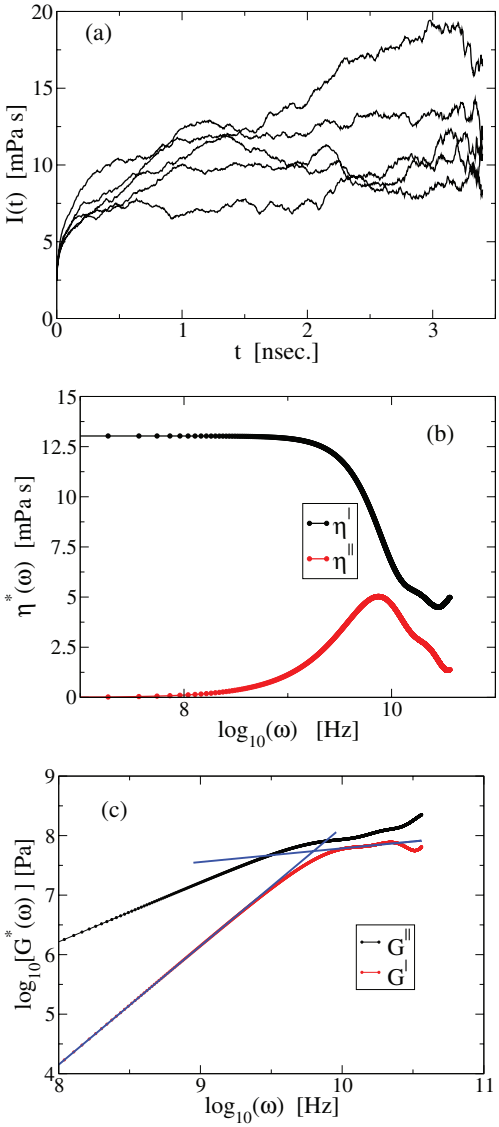

FIG. 8. For $T = 603$ K. (a) Running integral $I(t) = \int_0^t C_P(s)\, ds$ of the stress autocorrelation function for five samples among the ten successive ones in a production run. (b) Frequency-dependent viscosity as a function of frequency. Data was averaged and a Hann window applied to the single data set prior to the numerical Fourier-Laplace transform. (c) The corresponding-frequency dependent shear modulus $G^*(\omega) = G'(\omega) + iG''(\omega) = i\omega\eta^*(\omega)$. The two blues lines are fits of the form $G' \propto \omega^2$ and $G' \propto \omega^{1/4}$.

the shear-stress autocorrelation function, a time comparable to the τ_c parameter of Eq. (5) if this fitting function is used. This observation is also discussed in Ref. 11 by Z & G, and in order to estimate the viscosity at lower temperatures they therefore used the Debye-Stokes-Einstein equation which relates the molecular orientation relaxation time to the viscosity. This relation, however, breaks down for highly viscous fluids characterized by heterogeneous dynamics.[37] We will therefore not use this methodology here, but extract the viscosity from Fig. 8(b) letting $\omega \to 0$ which then limits us to present the result for the highest temperature only. In order to compare the predicted viscosity with experimental data available for lower temperatures, we extrapolate these to $T = 603$ K. In Fig. 9, this is done for the standard SV11274-70/100 bitumen, which is measured in this work (see Ref. 29 for a short

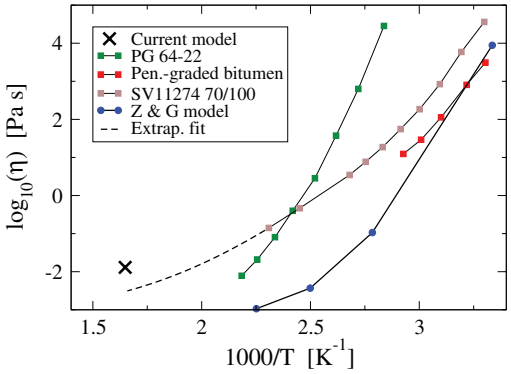

FIG. 9. Comparison of the zero-frequency viscosity (red circles) with experimental data (filled squares).[29] The predictions from Z & G's paper are also shown (blue circles connected with line). Data for PG 64-22 and penetration-graded bitumen was extracted from Ref. 11.

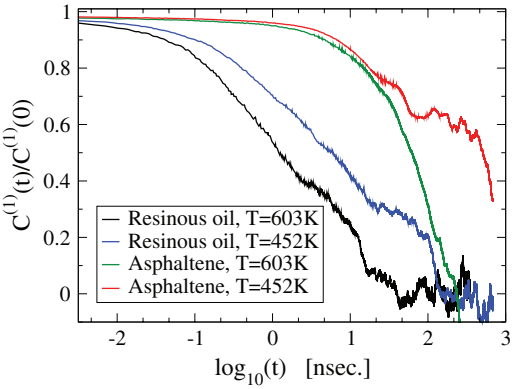

FIG. 11. Rotational correlation function $C^{(1)}$ for small times.

description of the measurement technique). We first note the well-known fact that the data are non-Arrhenius, since at high temperatures the viscosity must be close to 1 mPa s. Such a non-Arrhenius temperature dependence is found for most glass-forming liquids.[38] The model predicts the viscosity reasonably well for SV11274-70/100 bitumen, but not for PG 64-22 bitumen. The fact that the model predicts a bit higher viscosity can be linked to the high pressure of this state point. Moreover, as we mentioned above it is not the purpose of the model to fit a specific bitumen, and that the model cannot capture the dynamical properties of different bitumens is of course not surprising. Note that we used the stress autocorrelation function to calculate the viscosity, which is only possible for high temperatures. Other approximate methods[11,39] may be used to estimate the viscosity; however, it is not clear whether these methods can be applied to bitumen mixtures.

C. Rotational dynamics

It was observed above that while the molecular mean-square displacements indicate a well-defined diffusive regime for all temperatures studied except for the glassy state at $T = 301$ K, the stress autocorrelation functions showed a not fully relaxed system for times around 0.17 μsec. To better understand this behavior of the model, we also study the single molecule rotational dynamics for resinous oil and asphaltene. Rotation is quantified through the dynamics of the normalized orientational vector $\mathbf{u}(t)$ normal to one of the ring structures. As in Sec. II, the vector is defined as the cross product of two vectors pointing along a chemical bond as illustrated in Fig. 2, where the numbers indicate the atom indices involved in the definition of $\mathbf{u}$.

In Fig. 10, projections of the orientational vector are plotted as it evolves over time. It is evident that the smaller resinous oil molecules go through all possible orientations (to a good approximation) for all temperatures within the 0.85–1.75 μsec sample time. This is not the case for the larger asphaltene molecules. For lower temperatures, in particular, the orientation of this molecule is confined to a small subset of orientations. Naturally, this subset increases as a function of time.

The first-order rotational correlation function, $C^{(1)}(t) = \langle \mathbf{u}(0) \cdot \mathbf{u}(t) \rangle$,[30] is plotted in Fig. 11. The rotational relaxation appears to be governed by multiple relaxation times because of the nonsymmetric molecular structures. From

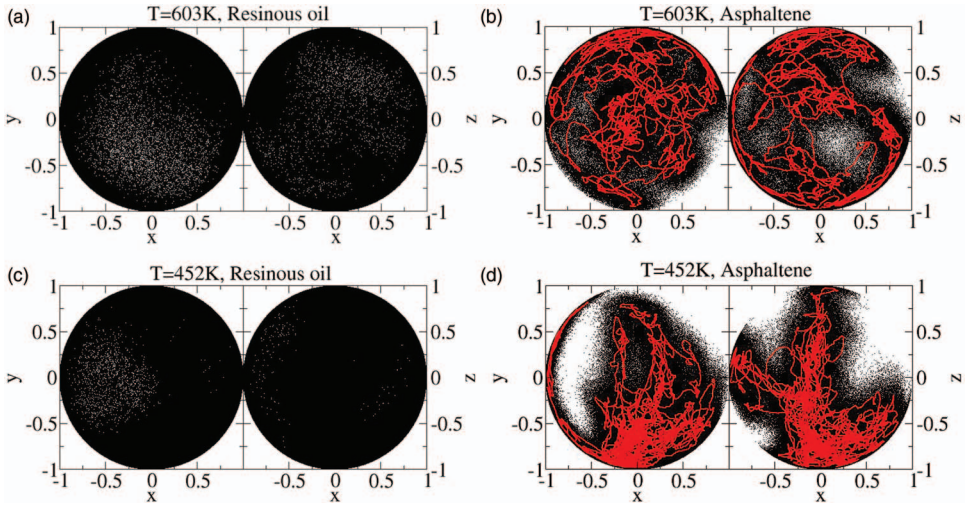

FIG. 10. Projections of the normalized orientation vector $\mathbf{u}$ as a function of time. Each dot represents the end point of the vector. For the asphaltenes red lines are averages of 1000 data points.

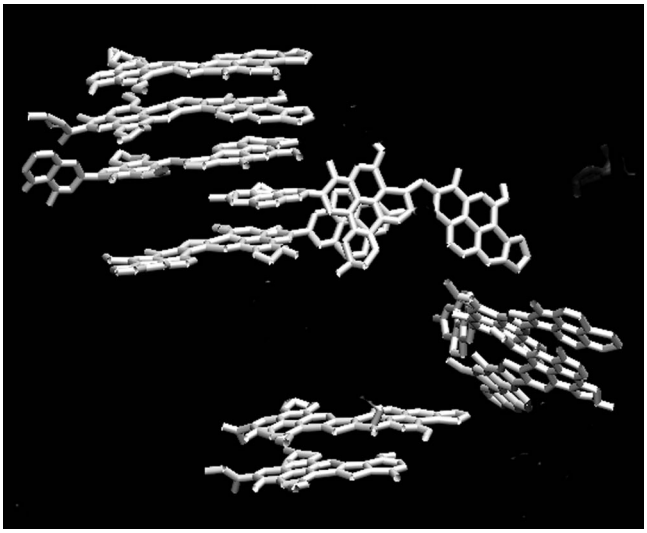

FIG. 12. Snapshot of the configuration of the asphaltenes. Only nine of the ten asphaltene molecules are shown for clarity.

$C^{(1)}(t)$, it is possible to define a characteristic relaxation time $\tau_r = \int_0^\infty C_r(t)\,dt/C_r(0)$. We obtain $\tau_r = 5$ ns for the resinous oil at 452 K. Again, this is evidence of a much slower dynamics compared to Z & G's model where $\tau_r = 1.44$ ns for the asphaltene at 443.15 K. In combination with Fig. 4, it can be concluded that while, on average, the asphaltene molecules exhibit the diffusive behavior, the single molecules keep their orientation relatively fixed. Such a decoupling between the rotational and diffusional dynamics is known from many experiments on viscous liquids, see Ref. 33 and references therein.

The snapshot shown in Fig. 12 highlights this picture; the asphaltene molecules tend to align and form "nano-aggregates,"[40,41] but occasionally they leave the aggregate and then later attach at a new position or aggregate. This dynamical behavior reveals that the diffusivity of the asphaltenes is determined by the mobility of just a small fraction of the molecules at any instant in time. The same remark applies to resin and resinous oil that also participate in the nano-aggregate formation. However, the dynamics of resin and resinous oil evolve at a different time scale. This long-time fixed orientation and clustering naturally leads to a very slowly decaying stress autocorrelation function. We conclude that the dynamics of the model is dominated by dynamical heterogeneities.

IV. SUMMARY

We have proposed a new molecular model of bitumen. Compared to Z & G's model, the dimethylnaphthalene molecules have been replaced by two higher-weight molecular structures representing resin and resinous oil molecules, respectively. The new "Cooee-bitumen" model is a united-atomic-unit model. This suppresses the high-frequency modes and makes possible longer simulation times than full-atom models. Using GPU-based software, we have demonstrated accessible time spans in order of μsec, rather than ns.[10] This makes it possible to study fairly slow relaxation processes characterizing bitumen and brings the models closer to real-life bitumen.

For the density and temperatures studied here, the model is characterized by a slow dynamics that changes little over a relatively large temperature range. The model predictions are in reasonable agreement with experimental data for diffusion and viscosity. Better agreement with specific bitumen solutions can be obtained by model re-parameterization and by choosing the state point carefully.

The model shows a heterogeneous dynamics deriving from the fact that the asphaltene, resin, and resinous oil molecules form nano-aggregates. Murgich *et al.*[4] and Z & G[10] have reported that asphaltene molecules tend to align, which supports this picture. The fact that asphaltene molecules form nano-aggregates is also known from experimental work.[40,41] The characteristic dynamical relaxation time of these localized aggregates is different from the more homogeneously distributed parts of the system, leading to a high degree of dynamical heterogeneity. In Fig. 5, one observes separate time scales, the slowest one due to the dynamics of larger asphaltene molecules. This indicates that the asphaltene nano-aggregate dynamics may be studied in more details on a longer time scale using coarse graining techniques like Brownian dynamics. This may form the foundation for a deeper understanding of the dynamical heterogeneity of bitumen. We plan to study this aspect of the model in future papers.

ACKNOWLEDGMENTS

This work was sponsored by the Danish Council for Strategic Research as part of the Cooee project ("CO_2 emission reduction by exploitation of rolling resistance modeling of pavements"). The centre for viscous liquid dynamics "Glass and Time" is supported by the Danish National Research Foundation's grant DNRF61.

[1] A. Wiehe and K. S. Liang, "Asphaltenes, resin, and other petroleum macromolecules," Fluid Phase Equilib. **117**, 201 (1996).
[2] E. Rogel and L. Carbognani, "Density estimate of asphaltenes using molecular dynamics simulations," Energy Fuels **17**, 378 (2003).
[3] L. Artok, Y. Hirose, Y. Su, M. Hosokawa, S. Murata, and M. Nomura, "Structure and reactivity of petroleum-derived asphaltene," Energy Fuels **13**, 287–296 (1999).
[4] J. Murgich, J. M. Rodriguez, and Y. Aray, "Molecular recognition and molecular mechanics of micelles of some model asphaltenes and resins," Energy Fuels **10**, 68–76 (1996).
[5] E. J. Barth, *Asphalt; Science and Technology* (Gordon and Breach, New York, 1962).
[6] L. Zhang and M. L. Greenfield, "Effect of polymer modification in properties and microstructures of model asphalt systems," Energy Fuels **22**, 3363–3375 (2008).
[7] *The Shell Bitumen Handbook*, 5th ed., edited by F. S. Rostler and D. Whiteoak (Shell UK Oil Products Limited, London, 2003).
[8] B. Schmidt and J. C. Dyre, "CO_2 emission reduction by exploitation of rolling resistance modelling pavements," Procedia Soc. Behav. Sci. **48**, 311 (2012).
[9] L. Zhang and M. L. Greenfield, "Analyzing properties of model asphalt using molecular simulation," Energy Fuels **21**, 1712–1716 (2007).
[10] L. Zhang and M. L. Greenfield, "Molecular orientation in model asphalt using molecular simulation," Energy Fuels **21**, 1102–1111 (2007).
[11] L. Zhang and M. L. Greenfield, "Relaxation time, diffusion and viscosity analysis of model asphalt systems using molecular simulation," J. Chem. Phys. **127**, 194502 (2007).
[12] L. Zhang and M. L. Greenfield, "Rotational relaxation times of individual compounds within simulations of molecular asphalt models," J. Chem. Phys. **132**, 184502 (2010).

[13]*CRC Handbook of Chemistry and Physics*, edited by D. R. Lide (CRC, Cleveland, 1976).
[14]R. L. Hubbard and K. E. Stanfield, "Determination of asphaltenes, oils, and resins in asphalt," Anal. Chem. **20**, 460 (1948).
[15]F. S. Rostler, "Fractional composition—Analytical and functional significance, bitominous materials: Asphalt, tars and pitches," in *Asphalts*, edited by A. J. Hoiberg (Wiley, 1965), Vol. 2.
[16]S. Toxvaerd, "Molecular dynamics calculation of the equation of state of alkanes," J. Chem. Phys. **93**, 4290 (1990).
[17]N. Bailey *et al.*, "RUMD: GPU-based molecular dynamics software" (unpublished), see http://rumd.org.
[18]F. S. Rostler and R. M. White, "Influence of chemical composition of asphalts on performance, particular durability," ASTM Spec. Tech. Publ. **277**, 64 (1959).
[19]ASTM, *1995 Annual Book of Standards: Method D* (American Society for Testing and Materials, Philadelphia, PA, 2007).
[20]F. D. Rossini, B. J. Mair, and A. J. Streiff, *Hydrocarbons from Petroleum: The fractionation, Analysis, Isolation, Purification and Properties of Petroleum Hydrocarbons* (American Petroleum Institute Research, 1953).
[21]D. A. Storm, J. C. Edwards, S. J. DeCanio, and E. Y. Sheu, "Molecular representations of Ratawi and Alaska North slope asphaltenes based on liquid- and solid-state NMR," Energy Fuels **8**, 561–566 (1994).
[22]W. L. Jorgensen and J. Tirado-Rives, "The OPLS potential functions for proteins, energy minimization for crystals of cyclic peptides and crambin," J. Am. Chem. Soc. **110**, 1657 (1988).
[23]See http://avogadro.openmolecules.net for Avogadro.
[24]J. Wang, R. M. Wolf, J. W. Caldwell, P. A. Kollman, and D. A. Case, "Development and testing of a general amber force field," J. Comput. Chem. **25**, 1157 (2004).
[25]R. Catlow, S. C. Parker, and P. Allen, *Computer Modelling of Fluids Polymers and Solids*, NATO ASI Series: Mathematical and Physical Sciences (Springer, 1989).
[26]S. Nosé, "A molecular dynamics method for simulation in the canonical ensemble," Mol. Phys. **52**, 255–268 (1984).
[27]W. G. Hoover, "Canonical dynamics: Equilibrium phase-space distributions," Phys. Rev. A **31**, 1695–1697 (1985).
[28]D. Frenkel and B. Smit, *Understanding Molecular Simulation* (Academic, London, 1996).
[29]The viscosity data for the straight run paving grade bitumen 70/100 (sample ID SV11274) are obtained by combining two measurement techniques. In the temperature range from 100 and down to 30 °C in successive step of 10 °C, the complex shear modulus is determined by a dynamic shear rheometer with frequency sweeps from 0.01 Hz to 10 Hz under constant strain amplitude similar to the principle described in European standard EN 14770. From the complex shear modulus and phase angle, the viscosity is calculated. At 135 °C and 180 °C, the Newtonian viscosity is determined by rotational viscometry using a co-axial cylinder system ("Brookfield") in accordance with European standard EN 13302. Further details can be found in E. Nielsen, *Rubber modified asphalt—Report on trial sections with rubber modified asphalt with the product ROAD+GENAN A/S)*, Danish Road Directorate, report no. 432, 2013.
[30]J. P. Hansen and I. R. McDonald, *Theory of Simple Liquids* (Academic, London, 2006).
[31]S. R. Upreti and A. K. Mehrotra, "Diffusivity of CO_2, CH_4, C_2 H_4, and n_2 in Athabasca bitumen," Can. J. Chem. Eng. **80**, 116 (2002).
[32]L. Berthier and G. Biroli, "Theoretical perspective on the glass transition and amorphous materials," Rev. Mod. Phys. **83**, 587 (2011).
[33]M. D. Ediger and Peter Harrowell, "Perspective: Supercooled liquids and glasses," J. Chem. Phys. **137**, 080901 (2012).
[34]J. H. Irving and J. G. Kirkwood, "The statistical mechanical theory of transport processes. IV. The equations of hydrodynamics," J. Chem. Phys. **18**, 817 (1950).
[35]B. D. Todd and P. J. Daivis, "Homogeneous non-equilibrium molecular dynamics simulations of viscous flow: Techniques and applications," Mol. Simul. **33**, 189 (2007).
[36]A. Cavagna, "Supercooled liquids for pedestrians," Phys. Rep. **476**, 51 (2009).
[37]M. T. Cicerone and M. D. Ediger, "Enhanced translation of probe molecules in supercooled oterphenyl: Signature of spatially heterogeneous dynamics?," J. Chem. Phys. **104**, 7210 (1996).
[38]T. Hecksher, A. I. Nielsen, N. B. Olsen, and J. C. Dyre, "Little evidence for dynamic divergences in ultraviscous molecular liquids," Nat. Phys. **4**, 737 (2008).
[39]R. B. Bird, R. C. Armstrong, and O. Hassager, *Dynamics of Polymeric Liquids* (Wiley, 1987).
[40]J. G. Erdman, T. F. Yen, and S. S. Pollack, "Investigation of the structure of petroleum asphaltene by x-ray diffraction," Anal. Chem. **33**, 1587–1594 (1961).
[41]O. C. Mullins, H. Sabbah, J. Eyssautier, A. E. Pomerantz, L. Barré, A. B. Andrews, Y. Ruiz-Morales, F. Mostowfi, R. McFarlane, L. Goual, R. Lepkowicz, T. Cooper, J. Orbulescu, R. M. Leblanc, J. Edwards, and R. N. Zare, "Advances in asphaltene science and the Yen-Mullins model," Energy Fuels **26**, 3986 (2012).